Quantitative Multiple-Quantum Magic-Angle-Spinning NMR Spectroscopy of Quadrupolar Nuclei in Solids

Gang Wu, David Rovnyak, and Robert G. Griffin*

Contribution from the Francis Bitter Magnet Laboratory and Department of Chemistry, Massachusetts Institute of Technology, Cambridge, Massachusetts 02139

Received May 3, 1996[⊗]

Abstract: We describe a new approach for observation of multiple-quantum (MQ) NMR spectra of $S = {}^3/_2$ nuclei with magic-angle spinning (MAS). The new method employs the *R*otation-*I*nduced *A*diabatic *C*oherence *T*ransfer (RIACT) that occurs between triple-quantum (3Q) and central-transition (1Q) coherences in $S = {}^3/_2$ systems. In contrast to currently available coherence-transfer techniques, RIACT is relatively insensitive to the magnitude of the quadrupole interaction for $e^2qQ/h \leq 4$ MHz for both 3Q excitation and 3Q-to-1Q conversion. Thus, RIACT provides a means of extracting quantitative information about site populations from isotropic MQ NMR spectra. We illustrate the utility of the approach with ^{23}Na ($S = {}^3/_2$) MQ NMR spectra of a series of sodium salts exhibiting crystallographically distinct sites. The spectra provide quantitative measurements of quadrupolar parameters, chemical shifts, and relative site populations for each of the crystallographically distinct sodium sites.

Introduction

Techniques for recording high-resolution nuclear magnetic resonance (NMR) spectra of spin-$^1/_2$ nuclei in solids are now well-developed and the spectra provide site-specific information about site populations, chemical bonding, and molecular structure.[1−5] In contrast, NMR methods for observing high-resolution spectra of half-integer quadrupolar nuclei ($S \geq {}^3/_2$) are in their infancy. Presently, several NMR approaches—magic angle spinning (MAS),[6,7] variable-angle spinning (VAS),[8,9] dynamic-angle spinning (DAS),[10,11] and double rotation (DOR)[12−14]—are used in the study of solids ranging from minerals to heme carbon monoxide complexes.[15−25] While these approaches are intellectually stimulating, they nevertheless yield spectra which consist of powder line shapes, require angle switching, or utilize probes with a low filling factor.

Recently, a new class of multiple quantum (MQ) MAS NMR experiments have been described,[26] which address these problems through the correlation of a specific MQ coherence with the central transition, yielding isotropic NMR spectra for half-integer quadrupolar nuclei. Using variations of this approach, several research groups have reported high-resolution NMR spectra of ^{23}Na ($S = {}^3/_2$), ^{17}O ($S = {}^5/_2$), ^{27}Al ($S = {}^5/_2$), ^{55}Mn ($S = {}^5/_2$), and ^{87}Rb ($S = {}^3/_2$) nuclei.[26−31]

A major problem with these MQ experiments is that both the excitation of MQ coherence and its conversion into observable single-quantum (1Q) coherence depend strongly upon the magnitude of the quadrupolar interaction. This has led to NMR spectra where crystallographically distinct sites give rise to isotropic lines whose intensities are significantly *different* from those expected on the basis of the site population. A case which illustrates this point concerns the ^{23}Na NMR spectra of anhydrous Na_2HPO_4 which has three crystallographically nonequivalent Na sites with relative populations of 1:1:2 with e^2qQ/h of Na(1) 1.37, Na(2) 2.13, and Na(3) 3.70 MHz, respectively.[32] In the original three-pulse MQ experiment[26] the

[⊗] Abstract published in *Advance ACS Abstracts,* September 1, 1996.

(1) Stejskal, E. O.; Memory, J. D. *High-Resolution NMR in the Solid State*; Oxford University Press: New York, 1994.
(2) Ernst, R. R.; Bodenhausen, G.; Wokaun, A. *Principles of Nuclear Magnetic Resonance in One and Two Dimensions*; Oxford University Press: Oxford, U.K., 1987.
(3) Diehl, P.; Fluck, E.; Günther, H.; Kosfeld, R.; Seelig, J., Eds. *NMR Basic Principles and Progress*; Springer-Verlag: Berlin, 1994; Vols. 30−33.
(4) Griffiths, J.; Griffin, R. G. *Anal. Chim. Acta* **1993**, *283*, 1081.
(5) Garbow, J. R.; Gullion, T. In *Carbon-13 NMR Spectroscopy of Biological Systems*; Beckmann, N., Ed.; Academic Press: San Diego, CA, 1995; Chapter 3.
(6) Andrew, E. R.; Bradbury, A.; Eades, R. G. *Nature* **1958**, *182*, 1659; **1959**, *183*, 1802.
(7) Lowe, I. J. *Phys. Rev. Lett.* **1959**, *2*, 285.
(8) Oldfield, E.; Schramm, S.; Meadows, M. D.; Smith, K. A.; Kinsey, R. A.; Ackerman, J. *J. Am. Chem. Soc.* **1982**, *104*, 919.
(9) Ganapathy, S.; Schramm, S.; Oldfield, E. *J. Chem. Phys.* **1982**, *77*, 4360.
(10) Llor, A.; Virlet, J. *Chem. Phys. Lett.* **1988**, *152*, 248.
(11) Mueller, K. T.; Sun, B. Q.; Chingas, G. C.; Zwanziger, J. W.; Terao, T.; Pines, A. *J. Magn. Reson.* **1990**, *86*, 470.
(12) Samoson, A.; Lippmaa, E.; Pines, A. *Mol. Phys.* **1988**, *65*, 1013.
(13) Chmelka, B. F.; Mueller, K. T.; Pines, A.; Stebbins, J.; Wu, Y.; Zwanziger, J.W. *Nature* **1989**, *339*, 42.
(14) Wu, Y.; Sun, B. Q.; Pines, A.; Samoson, A.; Lippmaa, E. *J. Magn. Reson.* **1990**, *89*, 297.
(15) Schramm, S.; Oldfield, E. *J. Am. Chem. Soc.* **1984**, *106*, 2502.
(16) Oldfield, E.; Kirkpatrick, R. J. *Science* **1985**, *227*, 1537.
(17) Farnan, I.; Grandinetti, P. J.; Baltisberger, J. H.; Stebbins, J. F.; Werner, U.; Eastman, M. A.; Pines, A. *Nature* **1992**, *358*, 31.
(18) Gann, S. L.; Baltisberger, J. H.; Wooten, E. W.; Zimmermann, H.; Pines, A. *Bull. Magn. Reson.* **1994**, *16*, 68.
(19) Dirken, P. J.; Smith, M. E.; Whitfield, H. J. *J. Phys. Chem.* **1995**, *99*, 395.
(20) Vosegaard, T.; Skibsted, J.; Bildsøe, H.; Jakobsen, H. J. *J. Phys. Chem.* **1995**, *99*, 10731.
(21) Grandinetti, P. J.; Baltisberger, J. H.; Farnan, I.; Stebbins, J. F.; Werner, U.; Pines, A. *J. Phys. Chem.* **1995**, *99*, 12341.
(22) Jarvie, T. P.; Wenslow, R. M.; Mueller, K. T. *J. Am. Chem. Soc.* **1995**, *117*, 570.
(23) Youngman, R. E.; Zwanziger, J. W. *J. Am. Chem. Soc.* **1995**, *117*, 1397.
(24) Fyfe, C. A.; Wong-Moon, K. C.; Huang, Y.; Grondey, H. *J. Am. Chem. Soc.* **1995**, *117*, 10397.
(25) Park, K. D.; Guo, K.; Adebodun, F.; Chiu, M. L.; Sligar, S. G.; Oldfield, E. *Biochemistry* **1991**, *30*, 2333.
(26) Frydman, L.; Harwood, J. S. *J. Am. Chem. Soc.* **1995**, *117*, 5367.
(27) Medek, A.; Harwood, J. S.; Frydman, L. *J. Am. Chem. Soc.* **1995**, *117*, 12779.
(28) Wu, G.; Rovnyak, D.; Sun, B. Q.; Griffin, R. G. *Chem. Phys. Lett.* **1996**, *249*, 210.
(29) Fernandez, C.; Amoureux, J. P. *Chem. Phys. Lett.* **1995**, *242*, 449.
(30) Fernandez, C.; Amoureux, J. P. *Solid State Nucl. Magn. Reson.* **1996**, *5*, 315.
(31) Massiot, D.; Touzo, B.; Trumeau, D.; Coutures, J. P.; Virlet, J.; Florian, P.; Grandinetti, P. J. *Solid State Nucl. Magn. Reson.* **1996**, *6*, 73.
(32) Baldus, M.; Meier, B. H.; Ernst, R. R.; Kentgens, A. P. M.; Meyer zu Altenschildesche, H.; Nesper, R. *J. Am. Chem. Soc.* **1995**, *117*, 5141.

S0002-7863(96)01467-9 CCC: $12.00

NMR peak corresponding to the Na(3) site was absent, and in our recent spectra with the two-pulse sequence[28] its intensity was approximately $^1/_3$ that of the Na(1) site, whereas it should have been twice as strong. Thus, with present methodology the signal intensities in the spectra do not reflect the relative populations of the individual sites. Since it is axiomatic that quantification of signal intensities in NMR spectra is crucial in applications to the analysis of inorganic, organic or biological materials, it is desirable to correct this deficiency.

In the present study, we describe a new method of observing high-resolution MQ spectra of $S = {}^3/_2$ nuclei which provides quantitative spectral intensities. The approach employs *R*otation-*I*nduced *A*diabatic *C*oherence *T*ransfer (RIACT) between triple-quantum (3Q) and central-transition coherences in $S = {}^3/_2$ systems undergoing MAS. The concept of 3Q $\leftrightarrow$ 1Q transfer in quadrupolar systems was first described by Vega,[33] and here we report direct experimental evidence for 3Q excitation via RIACT. Furthermore, we demonstrate that signal intensities in RIACT spectra are relatively *insensitive* to the magnitude of the quadrupole interaction, thus permitting quantitative measurements of site populations. We illustrate the new method with an analysis of ^{23}Na isotropic NMR spectra for a series of sodium salts exhibiting crystallographically distinct sodium sites.

Experimental Section

Solid-State NMR. All sodium salts studied in this work were obtained from Mallinckrodt, Inc. and the solid-state NMR experiments were performed on a custom-designed NMR spectrometer operating at 105.22 MHz for ^{23}Na nuclei. The MAS probe was equipped with a 5-mm spinner assembly (Doty Scientific, Inc., Columbia, SC), and typical spinning speeds were 5−10 kHz. In the ^{23}Na NMR experiments, the radio frequency field strengths were 80 kHz, corresponding to ^{23}Na 90° pulse lengths of ≈3.1 μs. A sample of solid sodium bromide was used to align the magic angle (using ^{79}Br NMR signals) and to calibrate the radio frequency field strength at the ^{23}Na NMR frequency. More detailed experimental parameters are given in the figure captions.

Numerical Simulations. In the present study, all theoretical results were based upon numerical evaluation of the spin density matrix and were performed on an Alphastation 400 4/233 (Digital Equipment Corp.) using the NMRLAB program package.[34]

Rotation-Induced Adiabatic Coherence Transfer (RIACT)

In the rotating frame, the spin Hamiltonian for an $S = {}^3/_2$ nucleus in a strong magnetic field and an on-resonance spin-locking radio frequency field can be written as:[33]

$$H = \omega_1 S_x + (Q/2)[S_z^2 - S(S+1)/3] \qquad (1)$$

where Q is the first-order quadrupole splitting and ω_1 is the radio frequency field strength in angular frequency units. For a static solid, Q has the following form:

$$Q = (\omega_Q/2)(3\cos^2\theta - 1 - \eta\sin^2\theta\cos^2\phi) \qquad (2)$$

where

$$\omega_Q = 3e^2qQ/[2S(S-1)\hbar] \qquad (3)$$

In eq 2, η is the asymmetry parameter, and θ and ϕ are the polar and azimuthal angles orienting the direction of the applied magnetic field in the principal-axis system of the electric-field-gradient (EFG) tensor. The eigenstates and eigenvalues of the spin Hamiltonian (eq 1) have been previously derived[35,36] and

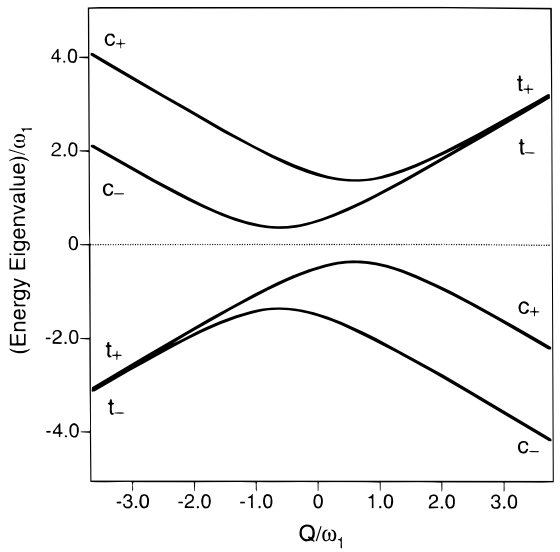

Figure 1. Energy level diagram for the spin Hamiltonian given in eq 1. When $|Q/\omega_1| \gg 1$, the eigenstates of the spin Hamiltonian are $|c_\pm\rangle$ and $|t_\pm\rangle$.

a typical energy level diagram is shown in Figure 1. If $|c_\pm\rangle = (|^1/_2\rangle \pm |-^1/_2\rangle)/2^{1/2}$ and $|t_\pm\rangle = (|^3/_2\rangle \pm |-^3/_2\rangle)/2^{1/2}$ are chosen as bases, the eigenstates of the Hamiltonian can be expressed as:[36]

$$\psi_1 = \sin\left(\theta_- + \frac{\pi}{3}\right)|t_+\rangle - \cos\left(\theta_- + \frac{\pi}{3}\right)|c_+\rangle \qquad (4a)$$

$$\psi_2 = \cos\left(\theta_- + \frac{\pi}{3}\right)|t_+\rangle + \sin\left(\theta_- + \frac{\pi}{3}\right)|c_+\rangle \qquad (4b)$$

$$\psi_3 = \cos\left(\theta_+ - \frac{\pi}{3}\right)|t_-\rangle + \sin\left(\theta_+ - \frac{\pi}{3}\right)|c_-\rangle \qquad (4c)$$

$$\psi_4 = -\sin\left(\theta_+ - \frac{\pi}{3}\right)|t_-\rangle + \cos\left(\theta_+ - \frac{\pi}{3}\right)|c_-\rangle \qquad (4d)$$

where

$$\tan 2\theta_- = -3^{1/2}Q/(4\omega_1 - Q) \qquad (5)$$

$$\tan 2\theta_+ = -3^{1/2}Q/(4\omega_1 + Q) \qquad (6)$$

Clearly, when $|Q| \gg \omega_1$, the eigenstates of the spin Hamiltonian are $|c_\pm\rangle$ and $|t_\pm\rangle$,[33] and populations in these states give rise to central-transition ($+^1/_2 \leftrightarrow -^1/_2$) and triple-quantum ($+^3/_2 \leftrightarrow -^3/_2$) coherences, respectively. When Q is comparable to ω_1, neither $|c_\pm\rangle$ nor $|t_\pm\rangle$ are eigenstates of the spin Hamiltonian.

Suppose that the density matrix of the initial spin state is $\rho(0) = I_x^{(23)}$ and that $|Q| \gg \omega_1$. As Vega showed,[33] since $I_x^{(23)}$ is characterized by populations of the wave functions, $|c_\pm\rangle$, which are eigenstates of the spin Hamiltonian given in eq 1, the spin system should remain in its original state, i.e., being "spin-locked". During MAS, the first-order quadrupole splitting, Q, becomes time dependent, so that the eigenstates of the spin Hamiltonian also change with time. Under such circumstances, the initial eigenstates of the spin Hamiltonian, $|c_\pm\rangle$, will not remain as eigenstates; therefore, the initial coherence, $I_x^{(23)}$, will be lost in the course of the spin-locking period. Assuming an axially symmetric EFG tensor ($\eta = 0$) for simplicity, the time-dependent first-order quadrupole splitting, $Q(t)$, can be expressed in the following form,[33]

(33) Vega, A. J. *J. Magn. Reson.* **1992**, *96*, 50.
(34) Sun, B. Q.; Griffin, R. G. To be submitted for publication.
(35) Wokaun, A.; Ernst, R. R. *J. Chem. Phys.* **1977**, *67*, 1752.
(36) Vega, S. *J. Chem. Phys.* **1977**, *68*, 5518.

$$Q(t) = (\omega_Q/2)[-2^{1/2} \sin 2\beta \cos(\omega_r t + \gamma) + \sin^2 \beta \cos(2\omega_r t + 2\gamma)] \quad (7)$$

where β is the angle between the unique axis of the EFG tensor for a particular crystallite and the sample rotation axis, γ is a rotation of the EFG tensor about the spinning axis, and ω_r is the sample spinning frequency. Note that $Q(t)$ has components which oscillate at ω_r and $2\omega_r$, respectively. If the changes of $Q(t)$ are *adiabatic*—slow enough so that the spin system remains in its eigenstates—then as $Q(t)$ reverses sign due to sample rotation, the eigenstates of the spin Hamiltonian are changed from $|c_+\rangle$ and $|c_-\rangle$ to $|t_+\rangle$ and $|t_-\rangle$, respectively.[33] Thus, the initial populations in $|c_\pm\rangle$ become populations in $|t_\pm\rangle$ accordingly. For crystallite orientations where the component oscillating at ω_r is predominant, the sign reversal of $Q(t)$ occurs twice per rotor period, τ_r. Thus, the initial coherence, $I_x^{(23)}$, is converted into the triple-quantum coherence, $I_x^{(14)}$, at $\tau_r/2$. It then returns to its original state at the end of a rotor cycle. So the following cycles occur during the spin-locking period:

$$\text{population transfer cycle: } |c_\pm\rangle \rightarrow |t_\pm\rangle \rightarrow |c_\pm\rangle \rightarrow \ldots$$

$$\text{coherence transfer cycle: } I_x^{(23)} \rightarrow I_x^{(14)} \rightarrow I_x^{(23)} \rightarrow \ldots$$

Similarly, if the initial coherence is $I_x^{(14)}$, it is converted to $I_x^{(23)}$ at $\tau_r/2$, and then returns to $I_x^{(14)}$ at τ_r. For crystallite orientations where the component oscillating at $2\omega_r$ is predominant, the aforementioned cycles occur twice per rotor period and therefore maximum $I_x^{(23)} \leftrightarrow I_x^{(14)}$ transfer occurs at $\tau_r/4$ and $3\tau_r/4$. The RIACT phenomenon for $S = {}^3/_2$ nuclei is conceptually identical to the well-known population inversion for two-level spin systems induced by adiabatic passage in continuous-wave NMR.[37] Based upon this concept, several NMR techniques have been recently developed in order to measure internuclear distances between spin-$^1/_2$ and quadrupolar nuclei.[38−43]

Vega[33] introduced an adiabaticity parameter, α, and defined the adiabatic condition as

$$\alpha = \frac{\omega_1^2}{\omega_Q \omega_r} \gg 1 \quad (8)$$

However, since the first-order quadrupole splitting is orientation dependent, eq 8 should not be treated as a strict constraint for the adiabatic condition. In other words, even when $\alpha \leq 1$, there is a significant portion of crystallites satisfying the adiabatic condition. Other definitions of the adiabaticity parameter are discussed by Hayashi[44] and by Baltisberger et al.[45]

The pulse sequences used for observing the RIACT phenomenon for $S = {}^3/_2$ nuclei are depicted in Figure 2. In Figure 2a is shown the standard spin-locking sequence where the initial central-transition coherence, $I_x^{(23)}$, is created by a phase-alternated 45° pulse (an effective 90° pulse for the central transition of $S = {}^3/_2$ nuclei) and the central-transition coherence is observed after the spin lock. To observe the evolution of the 3Q coherence as a function of the spin-locking time, τ_{SL}, an additional radio frequency pulse must be added at the end of τ_{SL} (see Figure 2b), so that the 3Q coherence can be converted to detectable central-transition coherence. It is also important to use the phase cycling that selects the coherence transfer pathway of $0 \rightarrow (-3) \rightarrow (-1)$.[26] Experimental results for solid $NaNO_2$ (**1**) are shown in Figure 3, together with numerical calculations where oscillatory behavior is observed for both the 1Q and 3Q coherences. It is important to emphasize that maximum 3Q excitation did not appear at $\tau_r/2$, but rather at $\tau_r/4$ and $3\tau_r/4$. This observation indicates that for a significant number of crystallites, $Q(t)$ changes sign four times in a rotor period. In fact, it can be readily shown from eq 7 that for one-third of the crystallites, $Q(t)$ reverses sign four times per rotor cycle. As we shall show later, setting τ_{SL} to $\tau_r/4$, instead of to $\tau_r/2$, always produces superior results. It should be mentioned that in Figure 3, the very rapid oscillation observed in the theoretical curve of the 1Q coherence is due to the $I_x^{(23)} \leftrightarrow I_z^{(23)}$ nutation and was not detected experimentally because of the τ_{SL} increments employed in the measurement. As seen in Figure 3, the experimental curves are well reproduced by numerical simulations.

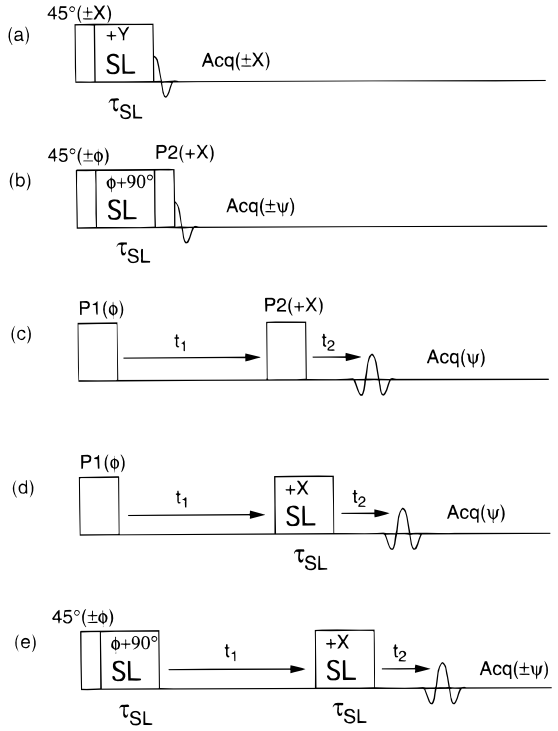

Figure 2. The pulse sequences used in this study. (a) Pulse sequence for spin-locking (SL) the central transition. (b) Pulse sequence for measuring the 3Q coherence created by RIACT during the spin-locking time. (c) The standard two-pulse (nutation) sequence for MQ experiments. (d) The RIACT(I) sequence for MQ experiments. (e) The RIACT(II) sequence for MQ experiments. See text for more discussions. In parts a−e, the phase-cycle schemes were as follows: $\phi = 0$, $\pi/6$, $2\pi/6$, ... $11\pi/6$; $\psi = 3(0, \pi/2, \pi, 3\pi/2)$. In parts d and e, the spin-locking time, τ_{SL}, was always set to $\tau_r/4$.

Clearly, the RIACT process provides an effective mechanism for 3Q ↔ 1Q transfer, and can be used either for generating 3Q coherence from the central-transition coherence or for converting 3Q to the central-transition coherence. More importantly, such 3Q ↔ 1Q transfers are expected to be independent of the magnitude of the quadrupole interaction,

(37) Abragam, A. *The Principles of Nuclear Magnetism*; Oxford University Press: Oxford, U.K., 1961; p 44.
(38) Grey, C. P.; Veeman, W. S. *Chem. Phys. Lett.* **1992**, *192*, 379.
(39) Grey, C. P.; Veeman, W. S.; Vega, A. J. *J. Chem. Phys.* **1993**, *98*, 7711.
(40) Grey, C. P.; Vega, A. J. *J. Am. Chem. Soc.* **1995**, *117*, 8232.
(41) Grey, C. P.; Eijkelenboom, A. P. A. M.; Veeman, W. S. *Solid State Nucl. Magn. Reson.* **1995**, *4*, 113.
(42) Gullion, T. *Chem. Phys. Lett.* **1995**, *246*, 325.
(43) Gullion, T. *J. Magn. Reson.* **1995**, *A117*, 326.
(44) Hayashi, S. *Solid State Nucl. Magn. Reson.* **1994**, *3*, 93.
(45) Baltisberger, J. H.; Gann, S. L.; Grandinetti. P. J.; Pines, A. *Mol. Phys.* **1994**, *81*, 1109.

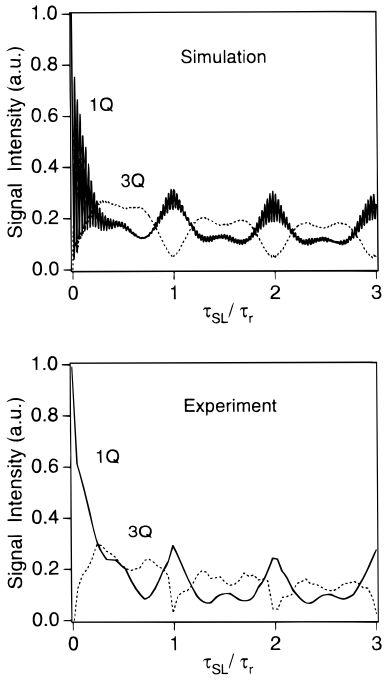

Figure 3. Calculated (top) and experimental (bottom) results for the oscillatory behavior of the ^{23}Na 3Q (dash line) and 1Q (solid line) coherences via RIACT in $NaNO_2$ (**1**). The sample spinning frequency was 3.13 kHz (the rotor period was $\tau_r = 319$ μs). The spin-locking radio frequency field strength was 62.5 kHz. The experimental increment for τ_{SL} was 15 μs. The quadrupole parameters of **1** used in the calculations are $e^2qQ/h = 1.1$ MHz and $\eta = 0.11$.

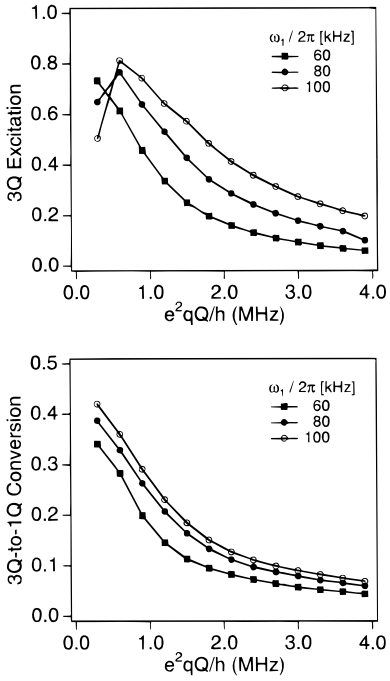

Figure 4. Calculated results for 3Q excitation (top) and 3Q-to-1Q conversion (bottom) by a nutation pulse as a function of e^2qQ/h at different radio frequency power levels. The sample spinning frequency was 10 kHz.

provided that the adiabatic condition is satisfied. This property of RIACT will be verified by numerical calculations presented in the following section.

Sensitivity of MQ Experiments

The pulse sequences used for MQ experiments are also depicted in Figure 2. Figure 2c is the standard two-pulse sequence for MQ experiments[27−30] where two nutation pulses are employed for 3Q excitation and 3Q-to-1Q conversion, respectively. The 3Q coherence created by the first nutation pulse is allowed to evolve for t_1, and then is converted to 1Q coherence for detection by the second nutation pulse. At the time $t_2 = kt_1$, where $k = {}^7/_9$ for $S = {}^3/_2$ nuclei, an echo will form. Sampling the top of the echo as a function of the total evolution time, $t_1 + t_2$, will yield a free-induction decay (FID) that consists of information about isotropic chemical shifts and isotropic second-order quadrupolar shifts, but is free of second-order quadrupolar broadenings.[26] The RIACT(I) sequence shown in Figure 2d utilizes a nutation pulse for 3Q excitation and a spin-locking pulse for 3Q-to-1Q conversion. As already discussed in the previous section, when τ_{SL} is chosen to be $\tau_r/4$, the 3Q coherence at the beginning of the spin-locking period will be converted into central-transition coherence by RIACT. In the RIACT(II) sequence, both 3Q excitation and 3Q-to-1Q conversion are achieved by RIACT. The first 45° pulse is used to create $I_x^{(23)}$, which is then converted to 3Q coherence via RIACT during the first spin-locking pulse. In the discussion that follows, we investigate how these three different pulse sequences depend upon the magnitude of the quadrupole interaction.

MQ Experiments by the Two-Pulse Sequence. It has long been known that MQ excitation efficiency from a nutation pulse depends strongly upon the magnitude of the quadrupole coupling constant.[36,46,47] When $\omega_Q \gg \omega_1$, the 3Q excitation for $S = {}^3/_2$ systems goes as ω_Q^{-2}.[36,46] We recently performed numerical calculations on the 3Q excitation from a nutation pulse as a function of both radio frequency power and quadrupole coupling constant.[28] Using a simplified model, Medek et al.[27] also evaluated the 3Q excitation and 3Q-to-1Q conversion by nutation pulses. All these previous studies indicated that both 3Q excitation and 3Q-to-1Q conversion efficiencies decrease substantially as the magnitude of the quadrupole coupling constant is increased. Here we present more complete results from numerical calculations about the sensitivity of the two-pulse nutation sequence as a function of the quadrupole coupling constant. As illustrated in Figure 4, both 3Q excitation and 3Q-to-1Q conversion decrease monotonically with the increase of the quadrupole coupling constant, except for very small quadrupole coupling constants, i.e., $\omega_Q < \omega_1$. Therefore, the peak intensities in MQ spectra obtained with the nutation method do not reflect directly the site populations. For a given e^2qQ/h value, both the 3Q excitation and 3Q-to-1Q conversion increase as the radio frequency field strength is increased; however, the 3Q excitation appears to be more sensitive to the radio frequency field strength. In addition, it is also clear from Figure 4 that the 3Q-to-1Q conversion is less efficient than the 3Q excitation. In fact, the low 3Q-to-1Q conversion efficiency is always a severe limiting factor in MQ experiments.

MQ Experiments by RIACT. As shown in the preceding section, the excitation efficiency and line intensities by the nutation method are strongly dependent on e^2qQ/h and therefore it is difficult to extract quantitative information about relative site populations from MQ spectra obtained with this approach. It is anticipated, however, that RIACT should be less sensitive to the quadrupole couplings provided that the adiabatic condition is approximately satisfied. Calculated results for the dependence

(46) Vega, S.; Naor, Y. *J. Chem. Phys.* **1981**, *75*, 75.
(47) Nielsen, N. C.; Bildsøe, H.; Jakobsen, H. J. *Chem. Phys. Lett.* **1992**, *191*, 205.

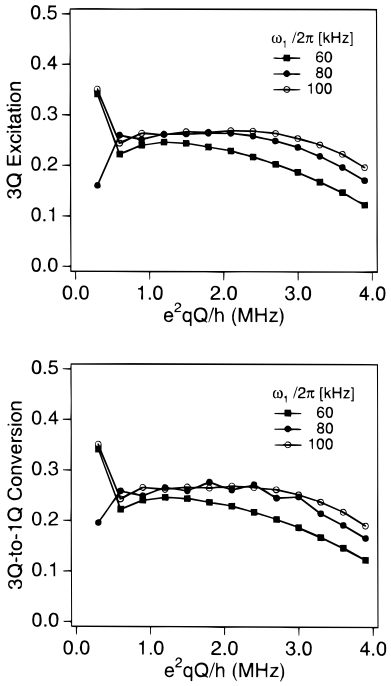

Figure 5. Calculated results for 3Q excitation (top) and 3Q-to-1Q conversion (bottom) by RIACT ($\tau_{SL} = \tau_r/4$) as a function of e^2qQ/h at different radio frequency power levels. The sample spinning frequency was 10 kHz.

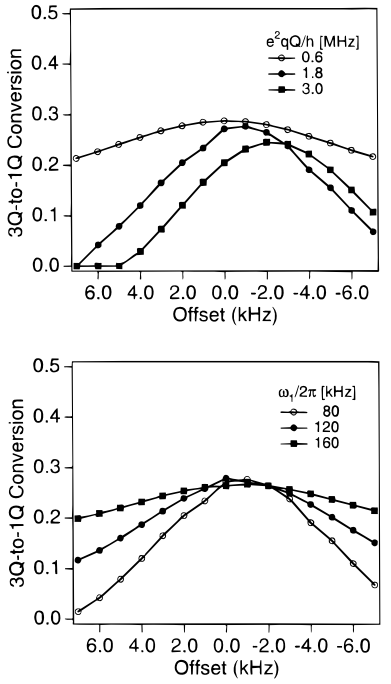

Figure 6. Calculated offset dependence of 3Q-to-1Q conversion by RIACT ($\tau_{SL} = \tau_r/4$) with different e^2qQ/h values (top) and with different spin-locking fields (bottom). Top: $\omega_1/2\pi = 80$ kHz. Bottom: $e^2qQ/h = 1.8$ MHz.

of RIACT upon the magnitude of e^2qQ/h are presented in Figure 5. Both the 3Q excitation and 3Q-to-1Q conversion processes are much less sensitive to variations of e^2qQ/h than those from the nutation method. For example, on varying e^2qQ/h from 1.0 to 3.6 MHz (typically found for ^{23}Na), the 3Q excitation by RIACT ($\tau_{SL} = \tau_r/4$ and $\omega_1/2\pi = 100$ kHz) is attenuated by less than 20%. In contrast, over the same range of e^2qQ/h, the 3Q excitation by the nutation method is attenuated by approximately a factor of 4 (see Figure 4).

Four additional points should be mentioned about Figure 5. First, superior results are always obtained for $\tau_{SL} = \tau_r/4$. In contrast, for $\tau_{SL} = \tau_r/2$, the numerical calculations indicate that both 3Q excitation and 3Q-to-1Q conversion efficiencies decrease significantly in the range of $e^2qQ/h = 2.5-4.0$ MHz. Second, compared with the results from the nutation method (Figure 4), RIACT exhibits substantially higher 3Q-to-1Q conversion efficiency, but somewhat lower 3Q excitation efficiency. Therefore, the RIACT(II) sequence is capable of providing reliable information about site populations and the RIACT(I) sequence should have the best sensitivity in terms of signal-to-noise ratio. Third, the calculated curves for 3Q excitation and 3Q-to-1Q conversion via RIACT are approximately identical. This is a consequence of the symmetry of RIACT. Finally, for larger e^2qQ/h values, a smaller fraction of crystallites satisfy the adiabatic condition, and therefore the overall RIACT efficiency declines.

As Vega noted previously,[33] the RIACT process between 3Q and 1Q coherences is also sensitive to resonance off-sets. In particular, an off-resonance radio frequency field would convert $I_x^{(23)}$ to $I_z^{(14)}$ rather than to the 3Q coherence, $I_x^{(14)}$, because, under the off-resonance condition, $|t_+\rangle$ and $|t_-\rangle$ are no longer the eigenstates of the spin system. Potentially, this could be a severe limitation of the RIACT method. However, it should be noted that the first-order degeneracy of the two eigenstates, $|t_+\rangle$ and $|t_-\rangle$, is actually lifted by the presence of the spin-locking field;[36] therefore, $|t_+\rangle$ and $|t_-\rangle$ will remain as eigenstates of the system provided that the resonance offset, $\Delta\omega$, is smaller than the energy difference between $|t_+\rangle$ and $|t_-\rangle$, i.e.,

$$\Delta\omega < \frac{3}{2}\left(\frac{\omega_1}{\omega_Q}\right)^2 \omega_1 \qquad (9)$$

To fully understand the limitations of the RIACT method arising from the resonance offset effect, we carried out extensive numerical calculations, the results of which are presented in Figure 6. As expected, the 3Q-to-1Q conversion efficiency is decreased as the resonance offset increases. Again, compared to $\tau_{SL} = \tau_r/2$, $\tau_{SL} = \tau_r/4$ is found to be a better choice since it is less sensitive to the resonance offset. It is also noted in Figure 6 that for larger e^2qQ/h values, the maxima are shifted to the lower frequencies, as a result of the second-order quadrupole shift. Therefore, if there are several sites present in a sample, it is recommended that the spin-locking field be set approximately to the center of the powder line shape arising from the site with the largest quadrupole coupling constant. A striking feature of the results shown in Figure 6 is that with high spin-locking fields, the 3Q-to-1Q efficiency becomes much less sensitive to the resonance offset, a result in agreement with the prediction of eq 9. Based upon the numerical calculations, it can be concluded that, for $e^2qQ/h < 3.0$ MHz, the reduction in 3Q-to-1Q conversion efficiency arising from a resonance offset of 4 kHz (corresponding to 38 ppm for ^{23}Na nuclei at 9.4 T) is less than 10%. With a spin-locking field of 160 kHz, however, the RIACT method can be extended to handle an offset range of more than 12 kHz.

Results and Discussion

^{23}Na NMR spectra of solid $Na_4P_2O_7 \cdot 10H_2O$ (**2**) are shown in Figure 7. The static ^{23}Na NMR spectrum (Figure 7a) and the X-ray crystal structure[48] of **2** suggest the presence of two crystallographically distinct Na sites with different quadrupole coupling constants. It is clear from the MAS spectrum of **2** that the Na(1) site has a much smaller quadrupole coupling constant than Na(2). The crystal structure of **2** indicates that one Na site is in an octahedral environment with six oxygen

Table 1. Quantitative Results from MQ ^{23}Na NMR Spectra of Sodium Salts

compd	site	e^2qQ/h (MHz)[a]	η[b]	δ_{iso} (ppm)[c]	site population analysis			
					theory[d]	nutation	RIACT(I)	RIACT(II)
$Na_4P_2O_7 \cdot 10H_2O$ (**2**)	Na(1)	$\leq$ 0.2		0.9	1	1.00	1.00	1.00
	Na(2)	2.00	0.2	4.8	1	0.12	0.45	0.87
$Na_3C_6H_5O_7 \cdot 2H_2O$ (**3**)	Na(1)	1.11	0.8	-3.3	1	1.00	1.00	1.00
	Na(2)	1.65	0.6	1.3	1	0.70	0.89	0.89
	Na(3)	1.75	0.6	7.0	1	0.49	0.66	0.86
Na_2HPO_4 (**4**)	Na(1)	1.31	0.2	4.5	1	1.00	1.00	1.00
	Na(2)	2.04	0.7	3.4	1	0.53	0.65	0.80
	Na(3)	3.84	0.3	8.8	2	0.31	0.62	1.93
$Na_2B_4O_7 \cdot 10H_2O$ (**5**)	Na(1)	0.58	0.0	10.7	1	1.00	1.00	1.00
	Na(2)	0.92	0.2	-1.3	1	0.81	1.36	1.25

[a] Errors are estimated to be $\pm$0.10 MHz. [b] Errors are estimated to be $\pm$0.1. [c] All ^{23}Na chemical shifts are relative to solid ^{23}NaBr. Errors in ^{23}Na chemical shifts are estimated to be $\pm$1.0 ppm. [d] From crystallographic symmetry.

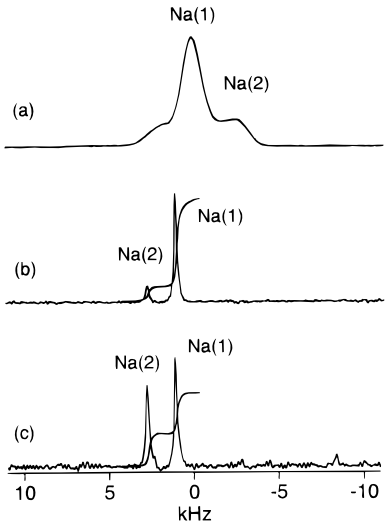

Figure 7. ^{23}Na NMR spectra of $Na_4P_2O_7 \cdot 10H_2O$ (**2**). (a) static, (b) MQ spectrum with the nutation sequence, and (c) MQ spectrum with the RIACT(II) sequence. In part b, the first and second nutation pulses were 6.0 and 2.5 μs, respectively. In part c, $\tau_{SL} = \tau_r/4 = 25.5$ μs. Other parameters used for obtaining each of the MQ spectra are as follows. The t_1 increment was 25.7 μs and a total of 128 t_1 increments were collected. For each t_1, 24 scans were recorded. $\omega_r/2\pi = 9.8$ kHz, RD = 2 s.

atoms from pyrophosphate groups, while for the other Na octahedron, two of the six oxygen atoms are from water molecules with rather long Na$\cdots$O distances.[48] Therefore, based upon the magnitude of the quadrupole coupling constants, Na-(1) is assigned to the Na site surrounded by six oxygen atoms from pyrophosphate groups.

In each of the ^{23}Na MQ spectra of **2** (Figure 7b and 7c), two well-resolved isotropic lines with widths of 180 Hz are observed. As Medek et al.[27] and Wu et al.[28] demonstrated, accurate information concerning chemical shifts and quadrupole parameters can be extracted directly from two-dimensional (2D) MQ spectra. From the 2D ^{23}Na MQ spectra of **2**, the following parameters were determined: Na(1), $\delta_{iso} = 0.9 \pm 1.0$ ppm, $e^2qQ/h \leq 0.2$ MHz; Na(2), $\delta_{iso} = 4.8 \pm 1.0$ ppm, $e^2qQ/h = 2.00 \pm 0.05$ MHz, $\eta = 0.2 \pm 0.1$. It is noted from Figure 7 that different line positions are observed in the static and MQ spectra. More specifically, whereas the signal from the Na(1) site is found to appear at higher frequency than that from Na-(2) in the static spectrum, it is at a lower frequency position in the MQ spectrum. Such changes of line position in MQ spectra have been previously discussed.[28]

According to the crystal structure of **2**,[48] the two Na sites are equally populated in the unit cell. However, in the ^{23}Na MQ spectrum obtained with the nutation method (Figure 7b), the line arising from the Na(2) site is of significantly less intensity than that from Na(1). The ratio of integrated area under the two lines is Na(1):Na(2) = 1:0.12. As noted above, this is due to the lower excitation efficiency of Na(2) which has a larger quadrupole coupling constant. With the RIACT(II) sequence, however, the two lines have approximately equal intensities, Na(1):Na(2) = 1:0.87 (Figure 7c). It is also worth noting that, as the isotropic peak intensity of Na(2) is enhanced by the RIACT sequence, the 2nd low-frequency rotational sideband associated with the Na(2) site (ca. -8.0 kHz) becomes observable.

To further test the applicability of the RIACT technique in obtaining quantitative MQ spectra, we investigated a series of sodium salts, each of which consists of crystallographically distinct Na sites with a wide range of quadrupole coupling constants. Detailed results from quantitative analysis of the ^{23}Na MQ spectra of trisodium citrate dihydrate, $Na_3C_6H_5O_7 \cdot 2H_2O$ (**3**), anhydrous Na_2HPO_4 (**4**), and $Na_2B_4O_7 \cdot 10H_2O$ (**5**) are listed in Table 1.

An excellent test sample is anhydrous Na_2HPO_4 (**4**), which is known to consist of three crystallographically distinct Na sites with different quadrupole coupling constants.[32] The ^{23}Na MQ spectra of **4** have also been reported recently with both the three-pulse[26] and the two-pulse sequences.[27,28] However, in all previously obtained ^{23}Na MQ spectra of **4**, the signal arising from the Na(3) site was either absent[26] or weak,[27,28] since the Na(3) site exhibits a relatively large quadrupole coupling constant, $e^2qQ/h = 3.70$ MHz.[32] This can be clearly seen in Figure 8b where the ^{23}Na MQ spectrum of **4** obtained with the nutation sequence consists of three isotropic peaks with the integral ratio Na(1):Na(2):Na(3) = 1.00:0.53:0.31. With the RIACT(I) sequence, both the Na(3) and Na(2) signals were enhanced. In addition, the signal-to-noise ratio of the MQ spectrum was also improved, as expected from the earlier discussions. With the RIACT(II) sequence, the integral ratio observed in the MQ spectrum becomes 1.00:0.80:1.93, approaching the ratio expected from the crystal structure of **4**,[32] Na(1):Na(2):Na(3) = 1:1:2. Similar to the case of **2**, significant intensity was observed at the 2nd low-frequency rotational sideband associated with the Na(3) site. The ^{23}Na quadrupole parameters and chemical shifts in **4** were determined from the 2D MQ spectra: Na(1), $\delta_{iso} = 4.5 \pm 1.0$ ppm, $e^2qQ/h = 1.31 \pm 0.10$ MHz, $\eta = 0.2 \pm 0.1$; Na(2), $\delta_{iso} = 3.4 \pm 1.0$ ppm, $e^2qQ/h = 2.04 \pm 0.10$ MHz, $\eta = 0.7 \pm 0.1$; Na(3), $\delta_{iso} = 8.8 \pm 1.0$ ppm, $e^2qQ/h = 3.84 \pm 0.10$ MHz, $\eta = 0.3 \pm 0.1$. These results are in agreement with those previously determined from DOR and MAS spectra of **4**.[32]

As seen from Table1, the RIACT(II) sequence is capable of yielding reasonably reliable information about relative popula-

(48) McDonald, W. S.; Cruickshank, D. W. J. *Acta Crystallogr.* **1967**, *22*, 43.

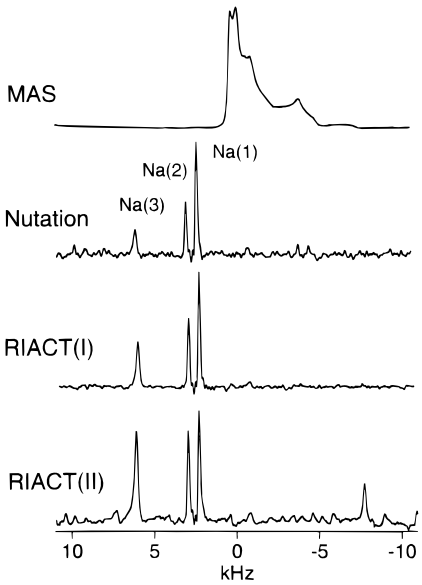

Figure 8. MAS and MQ ^{23}Na NMR spectra of anhydrous Na_2HPO_4 (**4**). For the MQ spectrum obtained by the nutation sequence, the two nutation pulses were 6.0 and 2.5 μs, respectively. For the spectra obtained by RIACT(I) and RIACT(II), $\tau_{SL} = \tau_r/4 = 20.5$ μs. In each of the MQ experiments, the t_1 increment was 25.7 μs, a total of 150 t_1 increments were collected, and for each t_1, 96 scans were recorded. $\omega_r/2\pi = 12.1$ kHz, RD = 2 s.

tions among crystallographically distinct sites. Two possible sources of error from the quantitative analysis of MQ spectra are worth mentioning. First, in order to prepare an initial spin state, $I_x^{(23)}$, that contains accurate site population information, a small excitation pulse,[49,50] instead of a 45° pulse, should be employed in the RIACT(II) sequence. However, this may attenuate the sensitivity of the MQ experiments. Second, if crystallographically distinct sites have different relaxation times in the rotating frame ($T_{1\rho}$), errors will be introduced into the peak intensities in MQ spectra, especially for long rotor cycles (*i.e.*, slow spinning speeds). In the present study, the spinning speeds are on the order of 10 kHz ($\tau_r/4 = 25$ μs), where the $T_{1\rho}$ effect is negligible for sodium salts.

(49) Samoson, A.; Lippmaa, E. *Phys. Rev.* **1983**, *B28*, 6567.

Conclusions

We have described a new method of obtaining MQ spectra for $S = {}^3/_2$ nuclei, from which complete quantitative information on relative site populations can be extracted. The new method is straightforward to implement and is relatively insensitive to the magnitude of the quadrupole interaction for $e^2qQ/h < 4$ MHz, which is the practical range of quadrupole coupling constants for ^{7}Li, ^{11}B, ^{23}Na, and ^{87}Rb nuclei. In addition, the RIACT method also enhances the sensitivity of MQ experiments over a large range of quadrupole coupling constants. We found that it is necessary to set the spin-locking time to $\tau_r/4$ rather than to $\tau_r/2$ in order to obtain the best experimental results. Possible extensions of the RIACT technique to MQ studies of half-integer quadrupolar nuclei with higher spin numbers such as $S = {}^5/_2$ are currently under investigation.

Acknowledgment. G.W. wishes to thank the Natural Sciences and Engineering Research Council (NSERC) of Canada for a postdoctoral fellowship. We are grateful to Mr. Chad Rienstra for building the MAS probe and to Dr. Boqin Sun for providing the NMRLAB program package. This research was supported by grants from the National Institute of Health (GM-23403 and RR-00995).

JA9614676

(50) Fenzke, D.; Freude, D.; Fröhlich, T.; Haase, J. *Chem. Phys. Lett.* **1984**, *111*, 171.